[1] **Junjian Chen**
[2,*] **Xinfei Huang**
[1] **Tiantian Cai**
[1] **Jie Shao**
[1] **Junye Li**
[3] **Yuzhou Ning**

# Traveling Wave Fault Localization Method Based on ICEEMDAN and DEO3S

Journal of Electrical Systems

***Abstract:*** - This paper proposes a fault localization method based on ICEEMDAN and DEO3S, which addresses the shortcomings of existing DC distribution network fault localization methods. The method employs the ICEEMDAN algorithm to adaptively decompose the fault voltage travelling wave signal at both ends of the current limiting reactor. The fault line is used to identify the main frequency component of the fault travelling wave, which is then extracted using the DEO3S algorithm to determine the precise moment when the fault travelling wave head arrives. This enables the fault point to be located with greater precision. The effectiveness of the fault location method is verified. A 10kVDC distribution line model was constructed using PSCAD/EMTDC to simulate various fault conditions. The results of this simulation demonstrate that the proposed method exhibits high accuracy in fault location, effectively mitigates the impact of random noise and initial travelling wave arrival time on location results, and exhibits high reliability.

***Keywords:*** DC distribution network, traveling wave, fault localization

## I. INTRODUCTION

In light of mounting environmental pressures and dwindling fossil fuel resources, China is endeavoring to transition from traditional fossil energy sources to cleaner energy sources, including wind and solar. The widespread adoption of cleaner energy sources represents a pivotal aspect of future energy strategies [1-2]. In its 2021 white paper, the Southern Power Grid sets out its goal of building a new type of power system, emphasizing the importance and promotion of multi-terminal DC technology [3-4]. Among these, flexible DC distribution lines have low loss, strong compatibility, and good power quality, which is conducive to improving power transmission efficiency and promoting access to distributed power sources [5-6]. The development prospect is favorable [7]. While research and practice in flexible DC distribution grids continue to advance, the current technology and engineering practice in flexible DC distribution grids are still in the process of continuous exploration and progress. Additionally, there are still several challenges to be resolved, including the lack of a standardized system. A number of challenges remain to be addressed [8-10]. Consequently, there is an immediate necessity to investigate expedient and dependable protection and precise localization techniques to guarantee the secure and stable operation of DC distribution systems. The prevailing fault localization techniques for DC distribution networks encompass fault analysis, injection, traveling wave, and fault analysis methods [11].

Fault analysis is the study of the mathematical relationship between the faulted electrical quantity and the fault location. This is achieved by means of circuit equations, such as current differentials [12] and harmonic impedance [13], and other electrical quantity characteristic information, which are used to calculate the exact location of the fault. In the literature [14], the transient current and voltage of the transient discharge process of the capacitor on the DC side have been employed for fault ranging. This method has the advantage of not relying on the "sampling frequency," and it has a "strong ability to adapt to changes in the transition resistance." However, this method can only be applied to double-ended power supply systems, and it cannot be used in multi-terminal ring DC distribution networks. The literature [15] employs an RL model to construct a fault location strategy for DC lines. However, the practical application of this strategy using differential calculation may result in significant errors and poor noise resistance. Literature [16] has also attempted to localize faults by studying the relationship between fault location and the amplitude and frequency of fault voltage oscillations. However, this method is only applicable to single DC lines and is challenging to implement in multi-terminal DC distribution systems.

In the injection method, an injection device is usually installed to actively inject signals into the system, and then the detected signals are used as the basis for fault localization [17]. In literature [18], an oscillating discharge

[1] China Southern Power Grid Digital Grid Research Institute Co., Ltd., Guangzhou, 510555, China
[2] State Key Laboratory of Disaster Prevention and Reduction for Power Grid, Changsha University of Science and Technology, Changsha, 410114, China
[3] China energy construction group Hunan Electric Power Design Institute Co. , Ltd, Changsha, 410076, China
* Corresponding author's e-mail: csusthxf@stu.csust.edu.cn

circuit is constructed by connecting capacitors in series, and then the frequency and attenuation of the discharge current are detected to locate the fault. In literature [19], a corresponding ranging module was designed according to different fault types to form a second-order RLC discharge loop, and fault ranging was realized by detecting the relevant characteristics of the discharge loop. These two methods are highly reliable and tolerant to transition resistance, but there is a localization dead zone at the proximal end. Therefore, literature [20] proposes a fault localization method by injecting a triangular wave of specific frequency and amplitude, based on the relationship between the frequency domain impedance of the characteristic signal and the fault location, which solves the problem of the existence of dead zones at the proximal end. However, this method requires the design of the injection device according to the line parameters and a suitable injection point, which has a high economic cost.

At present, in DC distribution network, the related research on fault localization still adopts the idea of AC distribution network, which does not fully consider the capacity of the converter and the extremely short time window of fault transient information in DC distribution network. In addition, the additional injection equipment is less economical and difficult to be widely used in the actual DC distribution network. The traveling wave method locates faults by measuring the arrival time of the traveling wave head [21]. Literature [22] proposed a wave-head calibration method based on mathematical morphology and realized fault localization on DC transmission lines using traveling wave theory. Literature [23] performs fault localization by calculating the time difference between the arrival of the voltage first traveling wave and the counter traveling wave. All these methods can effectively locate the fault without interference, but they do not consider the interference of external factors, especially in the case of large noise, the traveling wave head is difficult to be accurately calibrated, and the fault localization accuracy will be greatly reduced or even the localization failure will occur.

To address the above problems, literature [24] proposes a DC distribution network fault localization method based on gray comprehensive correlation, by analyzing the similarity of the traveling waveforms at the first and last ends of the line to solve the optimal time shift, so as to obtain the time difference between the arrival of the traveling waveforms at the first and last ends of the line for fault localization, which does not need to calibrate the traveling wave-head, and will not be unable to complete the fault localization because of the large noise. However, the similarity of this method will also be affected by the noise, and when the noise is large, it may lead to the inaccuracy of the optimal time shift, which will lead to a large localization error. Literature [25] proposed a high-voltage DC transmission line fault ranging method based on wavelet transform and ESMD algorithm, which improves the noise resistance of traveling wave localization method to a certain extent, and the proposed method has better localization accuracy and the ability to withstand transition resistance. However, the lack of reliability of wavelet transforms on large scale leads to the problem of modal aliasing of the method, and it is still difficult to accurately remove the noise in the case of large noise.

Literature [26] proposed a traveling wave ranging method based on traveling wave mode decomposition for double-ended traveling waves of UHV DC transmission lines, which uses Variational Mode Decomposition (VMD) to decompose the faulty traveling wave signals and the Teager Energy Operator (TEO) to the instantaneous energy spectrum calculated by the Teager Energy Operator (TEO) is used to prepare the calibrated traveling wave head. This method has strong robustness, can adapt to the large noise condition and high resistance fault condition, and the localization accuracy is within 1 km when the transition resistance is less than 100Ω, which has certain technical practical value in long-distance UHV DC transmission lines. However, since the VMD decomposition needs to select the corresponding parameters artificially, it is difficult to find the optimal parameter combination, which will affect the accuracy of localization, resulting in the localization accuracy of the method can't be applied to the DC distribution network.

In summary, for the problems of existing DC distribution network fault localization methods, this paper proposes a new DC distribution network fault localization method, which adopts the ICEEMDAN algorithm to adaptively decompose the fault voltage traveling wave signals at the two ends of the fault line current limiting reactor to obtain the main frequency component of the fault traveling wave, and then applies the DEO3S algorithm to extract the time-domain energy spectrum of this main frequency component to obtain the precise time of arrival of the fault traveling wave head, thus realizing the precise localization of the fault point. Then, the DEO3S algorithm is used to extract the time-domain energy spectrum of the main frequency component to obtain the precise moment of arrival of the fault traveling wave, thus realizing the precise positioning of the fault point.

## II. FREQUENCY BAND DECOMPOSITION OF DISTURBED TRAVELING WAVE SIGNALS

When the fault traveling wave signal arrives at the detection point, it generates a high-frequency mutation signal, and its mutation point corresponds to the moment when the traveling wave arrives at the detection point. Considering that the fault traveling wave signal is often accompanied by a large amount of noise when a fault occurs in the DC distribution network, it is necessary to first decompose the signal into frequency bands to extract the main frequency component of the fault traveling wave signal for fault localization. In this paper, ICEEMDAN is used to decompose the fault voltage traveling wave signal at both ends of the current limiting reactor to extract its main frequency component, which can retain the fault information to the maximum extent while removing most of the other frequency band noise, accurately extracting the characteristic information of the fault traveling wave signal, improving the quality of the wave-head, and improving the robustness and positioning accuracy of the localization algorithm.

ICEEMDAN algorithm is a noise analysis and processing algorithm which is improved on the basis of Empirical Mode Decomposition (EMD), and improves the continuity of adjacent frequency band signals by adding white noise, further eliminating the influence of mode aliasing and residual noise, and its algorithm steps are as follows:

(1) Gaussian white noise is added to the original signal:

$$X_1^{(i)} = x + e_1 E_1\left(w^{(i)}\right) \quad (i = 1, 2, \cdots, n) \tag{1}$$

Where: $x$ is the original signal; $e$ is the signal-to-noise ratio; $w^{(i)}$ denotes the ith added Gaussian white noise; $E_1(w)$ denotes the first IMF component of the noise after EMD decomposition.

(2) Calculate the first decomposition residue

$$r_1 = \left\langle X_1^{(i)} - E_1\left(X_1^{(i)}\right)\right\rangle \tag{2}$$

(3) Calculate the first modal component:

$$\mathrm{IMF}_1 = x - r_1 \tag{3}$$

(4) Using the recursive formula $IMF_q = x - r_q$, estimate the second residual as a series of $r_1 + \mathrm{e}_2 E_2(\omega^{(i)})$ means and define the second modal component $IMF_2$:

$$\mathrm{IMF}_2 = r_1 - \left\langle\left(r_1 + e_2 E_2\left(w^i\right)\right)\right\rangle \tag{4}$$

(5) Calculate the kth order residual r:

$$r_k = \left\langle X_k^{(i)} - E_k\left(X_k^{(i)}\right)\right\rangle \tag{5}$$

(6) Calculate the kth order modal component $IMF_k$:

$$\mathrm{IMF}_k = r_{k-1} - r_k \tag{6}$$

(7) Return to step 5 until all IMF components and residuals have been calculated.

After decomposing the traveling wave signal using ICEEMDAN, a series of IMF components can be obtained, with the first component having the highest instantaneous frequency and the components arranged in order of magnitude of the instantaneous frequency. Each component is a part of the original signal, and the sum of the components can be reconstructed as the original signal.

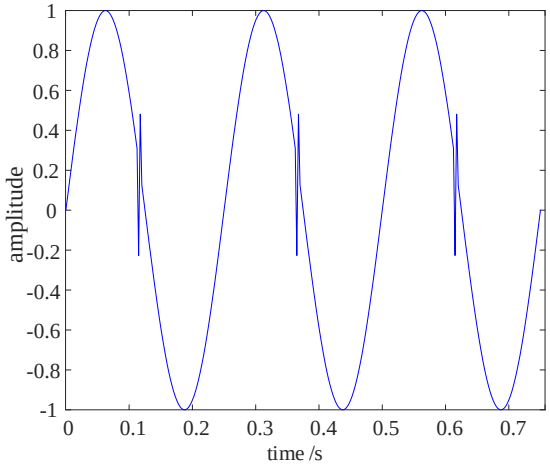


Figure 1: Simple Original Signal Diagram

In order to visualize the superiority of the ICEEMDAN algorithm compared to the EMD algorithm, the paper will compare and analyse to generate a section of the original signal synthesized by the low-frequency sinusoidal signals and intermittent high-frequency pulses as shown in Fig. 1, respectively, using the EMD algorithm and the ICEEMDAN algorithm to decompose the signals shown in Fig. 1, and the decomposition results are shown in Fig. 2 and Fig. 3, respectively:

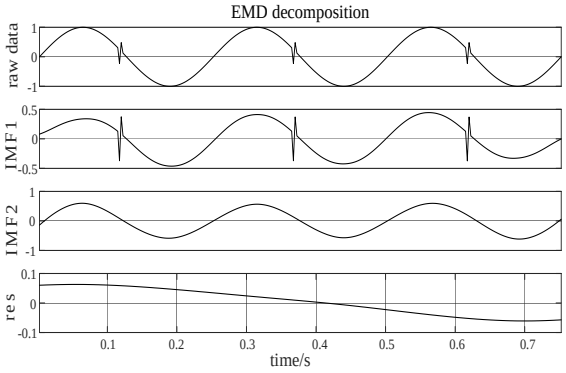


Figure 2: EMD decomposition result of simple original signal

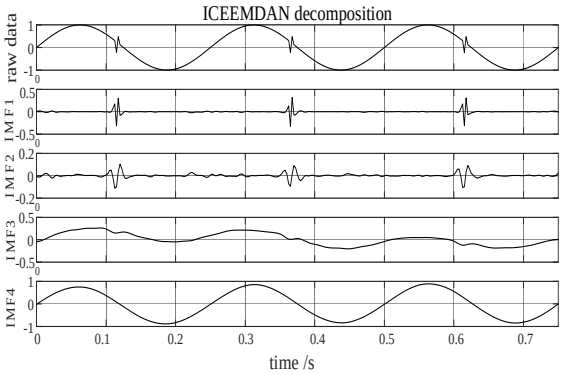


Figure 3: Results of ICEEMDAN decomposition of simple original signal

As can be seen from Fig. 2 and Fig. 3, for a mixed signal consisting of a low-frequency sinusoidal signal superimposed on an intermittent high-frequency pulse signal, the EMD decomposition shown in Fig. 2 does not accurately differentiate the low-frequency from the high-frequency signal, and its IMF1 component is still a low-frequency and high-frequency mixed signal, while its IMF2 component separates about half of the amplitude of the low-frequency component of the original signal, which is characterized by severe modal mixing, and it is not possible to effectively utilize the high-frequency transient information contained in the original signal. effectively utilize the high-frequency transient information contained in the original signal, and the decomposition effect is poor. The ICEEMDAN decomposition shown in Fig. 3 solves this problem by separating the high-frequency components of the original signal into its IMF1 and IMF2 components, while the IMF4 component corresponds to the low-frequency component of the original signal.

For traveling wave localization, ICEEMDAN decomposition can better capture the traveling wave features in the signal, decompose the non-smooth and non-linear traveling wave signal into smooth multiple local components, and to some extent, it can eliminate part of the noise and extract the fault feature signal for further analysis and processing. However, since the decomposed IMF components are all a function oscillating around zero, it is impossible to directly calibrate the moments corresponding to the traveling wave head, so it is necessary to adjust other algorithms to accurately calibrate the traveling wave head.

## III. WAVE-HEAD CALIBRATION FOR FAULTY TRAVELING WAVE SIGNALS

For the IMF components of different frequency bands after ICEEMDAN decomposition, the following qualitative analysis can be made: in each IMF component, the larger the proportion of fault transient information, the more concentrated its energy is, and the larger the proportion of noise, the more dispersed its energy is. Therefore, the peak-to-average energy ratio $K = \frac{\psi_{\max}}{\overline{\psi}}$ can be used to determine the main frequency component of the faulty traveling wave, and then this component can be used to calibrate the traveling wave head.

In practice, discrete TEOs are used to calculate the energy peak-to-average ratio, and the actual collected discrete current signal will be $x(n)$, and the energy value will be as shown in equation (7):

$$\psi(x(n)) = x^2(n) - x(n+1)x(n-1) \tag{7}$$

Due to the problem of large amplitude and frequency errors in the traveling wave fault localization using the TEO algorithm, this paper improves on this basis by adopting the DEO3S to calculate the energy value of each sampling point of the signal, and then identifies the wave-head through the corresponding instantaneous energy spectrum to achieve the effect of accurate fault localization.

DEO3S reduces the error and improves the noise immunity based on the TEO algorithm, expressed as

$$\varphi[x(n)] = \frac{\psi[x(n+1)] + 2\psi[x(n)] + \psi[x(n\text{-}1)]}{4} \tag{8}$$

where is the collected time signal, $\varphi[x(n)]$ is the instantaneous energy of the nth sample point, and $\psi[x(n)]$ is the TEO energy value of the nth sample point calculated by Eq. (7).

To illustrate the superiority of the DEO3S algorithm over the TEO algorithm, the signal shown in Fig. 1 is also used as the original signal for testing, and the corresponding instantaneous energy spectra are obtained by using the TEO and the DEO3S to compute the original signal, as shown in Fig. 4 and Fig. 5, respectively.

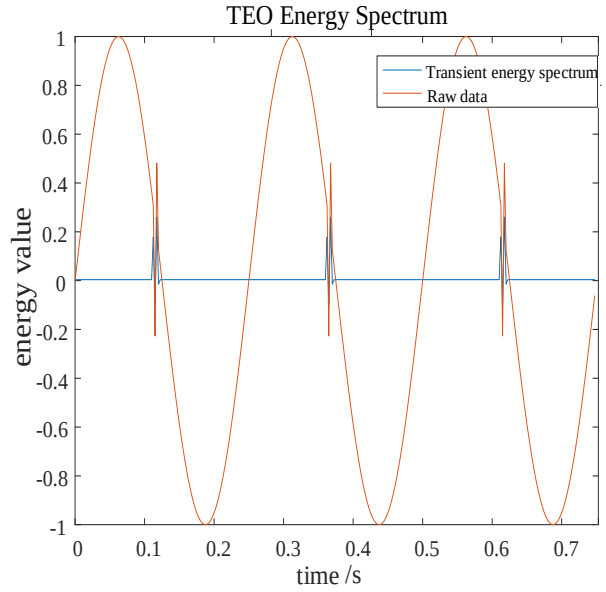


Figure 4: TEO calculation results for simple raw data

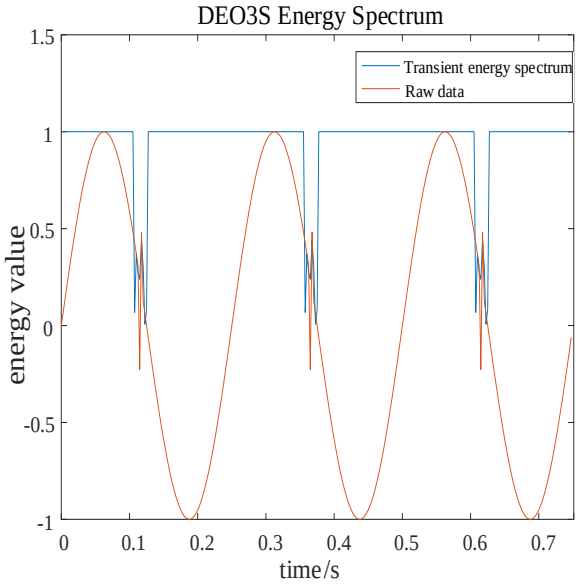


Figure 5: Results of DEO3S calculations for simple raw data

As shown in the figure, although the traditional TEO algorithm can calculate the energy value of intermittent high-frequency pulses, it ignores the energy of low-frequency sinusoidal signals and is only suitable for extracting the energy value of the highest frequency signal. The DEO3S algorithm can accurately calculate the energy of both low-frequency and high-frequency signals (the reason for the higher energy value of low-frequency signals is that the amplitude of low-frequency sinusoidal signals is much larger than that of high-frequency intermittent signals).

Due to the almost non-existence of industrial frequency AC signals in the DC distribution network, and by the influence of a large number of power electronic components in the system, the DC distribution network is more likely to generate high-frequency noise, so the use of TEO algorithm is susceptible to the interference of high-frequency noise, and the use of DEO3S algorithm can be better extracted fault transient information, with a stronger anti-noise ability and reliability.

Therefore, this paper adopts the DEO3S algorithm to calculate the energy peak-to-average ratio K value of each IMF component of the fault voltage traveling wave signal after decomposition, selects the IMF component with the largest K value as the main frequency component of the fault traveling wave, and constructs the corresponding instantaneous energy spectrum, and the corresponding moment of the horizontal axis at the point of the maximum value of energy in the vertical axis of the energy spectrum is calibrated to be the arrival moment of the first fault wave-head. The distance from the fault point to both ends of the line can be derived from the calibrated arrival times of the wave-heads at both ends of the line, thus completing the fault localization. This method is improved on the basis of the traditional method to achieve higher wave-head calibration accuracy and noise immunity.

## IV. FAULT LOCALIZATION METHOD BASED ON ICEEMDAN AND DEO3S

Due to the small amount of transient information that can be used for accurate fault location in the case of DC bipolar short-circuit faults, only the arrival time of the initial traveling wave head at both ends can be used for fault location. In this paper, by collecting the voltages of the current-limiting reactors at both ends of the faulted line, the traveling wave signal of the faulted voltage is subjected to frequency band decomposition based on ICEEMDAN to select the main frequency components, and then the corresponding transient energy spectra are constructed by using DEO3S to perform the calibration of the traveling wave head, which is used for accurate fault location by the principle of traveling wave localization at both ends.

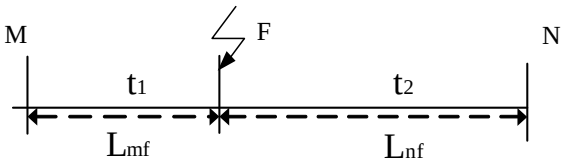


Figure 6: depicts a schematic diagram of double-ended traveling wave fault localization.

The principle of double-ended traveling wave fault localization is illustrated in Fig. 6. The expression for fault localization using double-ended wave-head information is as follows:

$$L_{\mathrm{mf}} = \frac{l + (t_1 - t_2)v}{2} \tag{9}$$

The moments at which the traveling wave head arrives at the M and N ends are designated as $t_1$ and $t_2$, respectively. The total length of the line is represented by $l$, the wave speed of the fault traveling wave is denoted by $v$, and $L_{mf}$ represents the length from the fault point F to the M end of the line.

Given that the length of the DC distribution network is considerably shorter than that of the DC transmission line, the small discrepancy in the traveling wave speed has a minimal impact on the absolute error of fault localization. Furthermore, the traveling wave speed in the overhead line is nearly equivalent to the speed of light. Consequently, in this paper, the traveling wave speed, denoted by $v$, is based on an empirical wave speed derived from the line parameters. The calibration of the arrival time of the wave head at both ends is accomplished through the ICEEMDAN decomposition of the faulty traveling wave signal. The main frequency component is then determined by DEO3S to extract its instantaneous energy spectrum, thereby enabling the accurate calibration of the traveling wave head. Following the calibration of the wave head, the arrival time of the wave head is substituted into Eq. (9) to complete the fault localization process. The schematic diagram of traveling wave fault localization is depicted in Fig. 7.

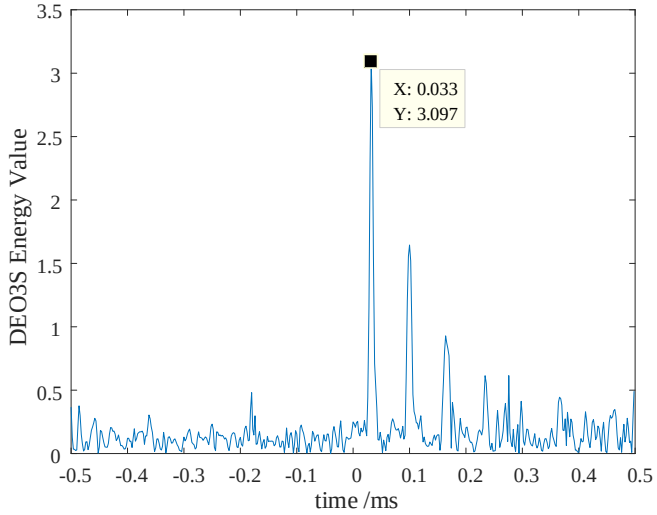


Figure 7： presents a schematic diagram of a traveling wave fault localization technique

As shown in Fig. 7, in the energy spectrum calculated by DEO3S, the X-axis coordinate of the first traveling wave head is calibrated to 0.033, which means that the arrival moment of the wave head is the 0.033 ms, and assuming that the fault occurs at the 0 ms and the traveling wave speed is the speed of light, the distance between the fault point and the measurement point can be calculated by the distance formula $L_{\mathrm{mf}} = t_1 v$ to be about 10 km. However, since the actual application cannot accurately know the exact time of fault occurrence, it is necessary to collect the traveling wave arrival moment t1 and t2 of the fault ends for traveling wave localization. However, since the actual application cannot accurately know the exact time of the fault occurrence, it is necessary to collect the traveling wave arrival moments t1 and t2 of the faulty double end to be used for traveling wave localization.

From Eq. (9), it can be seen that the main error of double-ended traveling wave localization comes from the moment $t_1$ and $t_2$ when the calibrated traveling wave head arrives at the two ends of the line, and the method proposed in this paper has a higher accuracy of the wave head calibration compared with the traditional method, For the double-ended timing error, a high-precision clock based on the Bei Dou/GPS can be used to reduce the timing error as much as possible to ensure the accuracy of fault localization.

The specific steps are as follows.

1) Install a traveling wave detection device at the first and last ends of the DC distribution line to detect the fault traveling wave signal.

2) Decompose the fault traveling wave using the ICEEMDAN algorithm to obtain multiple IMF components.

3) Calculate the instantaneous energy spectrum of each IMF component using DEO3S, select the IMF component with the highest peak-to-average energy ratio to be determined as the main frequency component, and use its instantaneous energy spectrum to calibrate the traveling wave head.

4) The corresponding moments of the highest energy points in the instantaneous energy spectra at both ends are calibrated as the arrival moments t1 and t2 of the faulty traveling wave.

5) The exact location of the fault point is calculated using the double-ended traveling wave localization formula given in Eq. (9).

In step 4), the calibration of the traveling wave head is carried out simultaneously at both ends of the fault line. At this juncture, it is not possible to ascertain the precise moment of the actual fault occurrence. Consequently, $t_1$ and $t_2$ do not represent the time of transmission of the fault traveling wave, but rather a specific moment. Given that the speed of transmission of the traveling wave in the overhead line is nearly that of light, a mere 1 μs of time error can result in a positioning error of nearly 300 m. Consequently, the sampling interval of the traveling wave fault location device is 1 μs, which corresponds to a sampling rate of. In order to determine the moment of arrival of the respective faulty traveling waves at the two ends of the line, it is necessary to use a sampling interval of 1 MHz. However, this is not compatible with conventional μs-level clock timing. Therefore, it is essential to install a Bei Dou/GPS satellite signal based on a high-precision clock in order to reduce the positioning error. It is imperative to install a high-precision clock based on Bei Dou/GPS satellite signals to minimize the positioning error.

The fault localization flowchart is shown in Fig. 8:

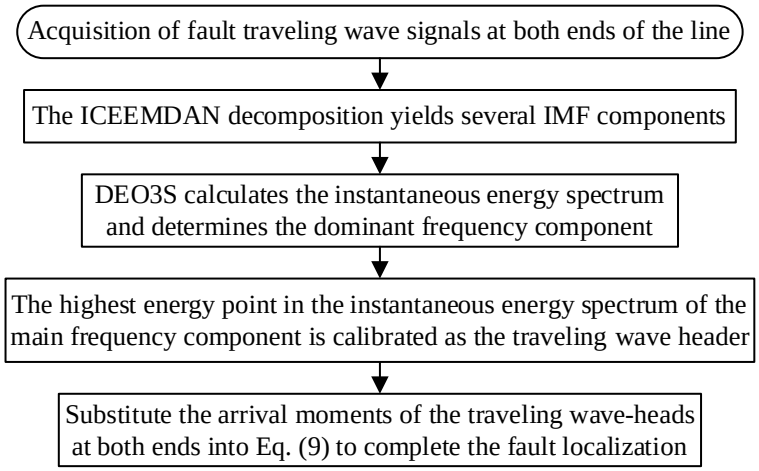


Figure 8: presents a flow chart illustrating the process of traveling wave fault localization

## V. SIMULATION VERIFICATION

### A. *Simulation Model*

The proposed fault localization method is validated using PSCAD/EMTDC, and a simulation model of a flexible DC distribution line is constructed as illustrated in Fig. 9. In this model, the traveling wave speed of the overhead line is $2.9829\times10^5$ km/s. The reference direction of the DC current is clockwise, and the reference direction of the voltage of the current-limiting reactor is aligned with that of the DC current.

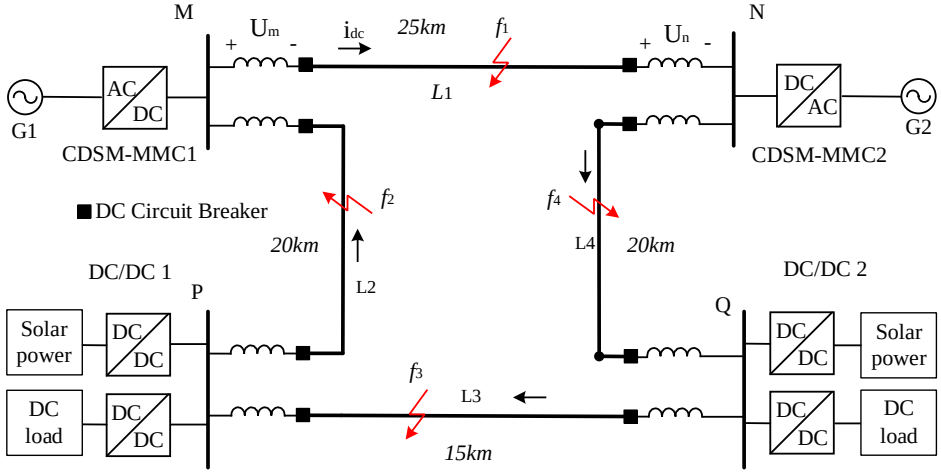


Figure 9: illustrates the structure of a multi-terminal ring flexible DC distribution grid with a voltage rating of ±10 kV

The specific parameters illustrated in Fig. 9 are presented in Table 1 and Fig. 10. The simulation sampling rate is set to 100 kHz, with the DC circuit breaker at the M end of the line depicted in the figure serving as the simulation test object.

Table 1: Parameters of the Converter Station

| Converter of Electric Current | Control Strategy | Voltage Ratio | Rated Capacity | Submodule Capacitance | Bridge Arm Reactors |
|---|---|---|---|---|---|
| CDSM-MMC1 | Constant Voltage | AC 10kV/ DC 10kV | 5MVA | 500μF | 15mH |
| CDSM-MMC2 | Constant Voltage | AC 10kV/ DC 10kV | 3MVA | 500μF | 15mH |
| DC/DC1 | MPPT | DC 10kV/ DC 750V | 4MVA | 500μF | / |
| DC/DC2 | MPPT | DC 10kV/ DC 750V | 2MVA | 500μF | / |

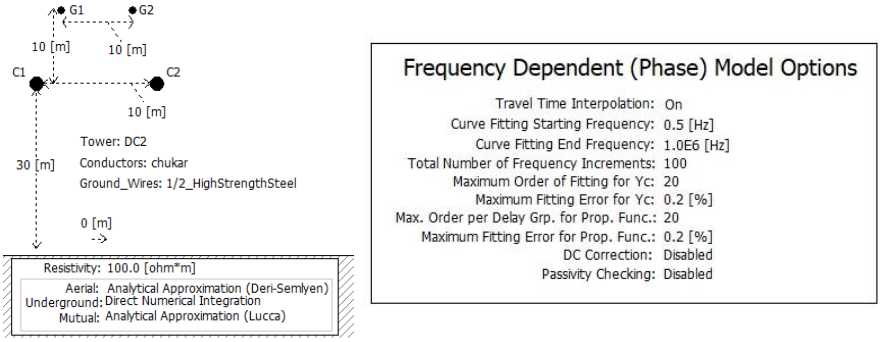


Figure 10: illustrates the DC line structure and associated parameters

The multi-terminal ring flexible DC distribution network, as illustrated in Fig. 9, is partitioned into four sections, designated as M, N, P, and Q. Each DC distribution line employs a frequency-dependent model, with a sampling frequency of 1 MHz. The proposed method for fault localization in DC distribution networks is based on the use of an instantaneous fast-action protection scheme for bipolar short-circuit faults. This scheme employs a data window length of 1 ms for protection calculations and a protection action time of within 1.5 ms. The method is unified in its approach and is therefore applied uniformly to the 1 ms time window data.

*B. Typical Failure Case Analysis*

In order to verify the feasibility of the proposed fault location method, a bipolar short-circuit fault is set up at F1 in Fig. 9 for simulation verification. The distance from the fault location to the M terminal is 15 km, and the transition resistance is 10 Ω. The results of the fault signal band decomposition indicate that the fault line is L1. To identify the fault location, the voltage traveling signals of the current-limiting reactors are collected from the M and N terminals. The measured voltages of the M and N terminals are shown in Fig. 11.

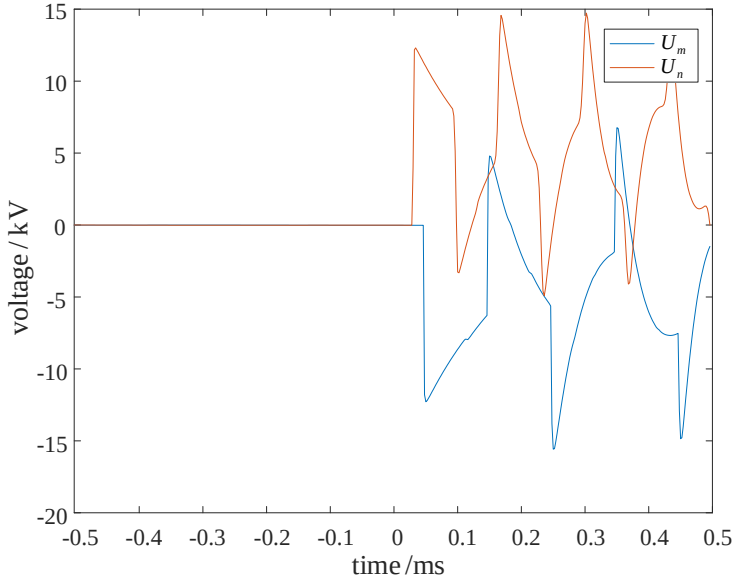


Figure 11: Voltage traveling wave signals measured by current-limiting reactors at M and N

As illustrated in Fig. 11, the current-limiting reactor of the DC distribution network effectively mitigates the fault current, yet its fault voltage exhibits a pronounced and discernible abruptness. In the absence of noise, multiple traveling wave-heads are discernible. In order to simulate the noise situation that may exist during a

real fault, 30 dB of noise is added to the signals measured at the M and N terminals in Fig. 11. The resulting voltage traveling wave signals are shown in Fig. 12.

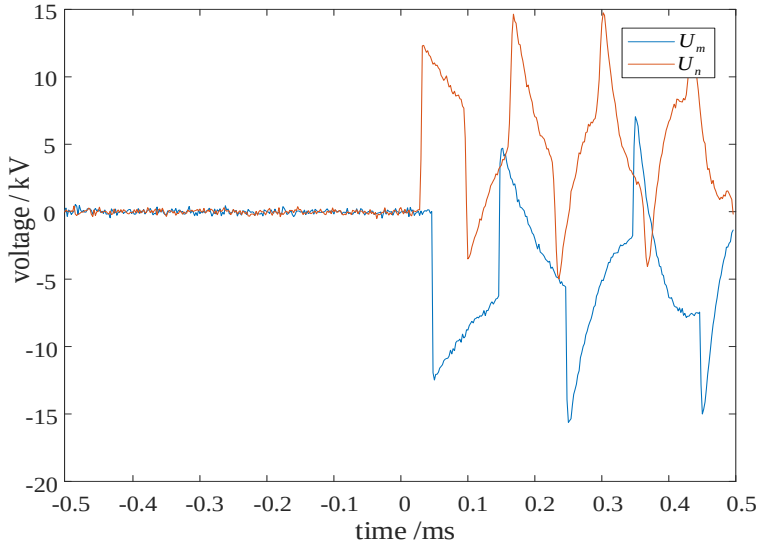


Figure 12: Voltage traveling wave signal with noise

As an illustrative example, the ICEEMDAN algorithm is employed to decompose the fault voltage traveling wave signal depicted in Fig. 12, with the resulting decomposition presented in Fig. 13.

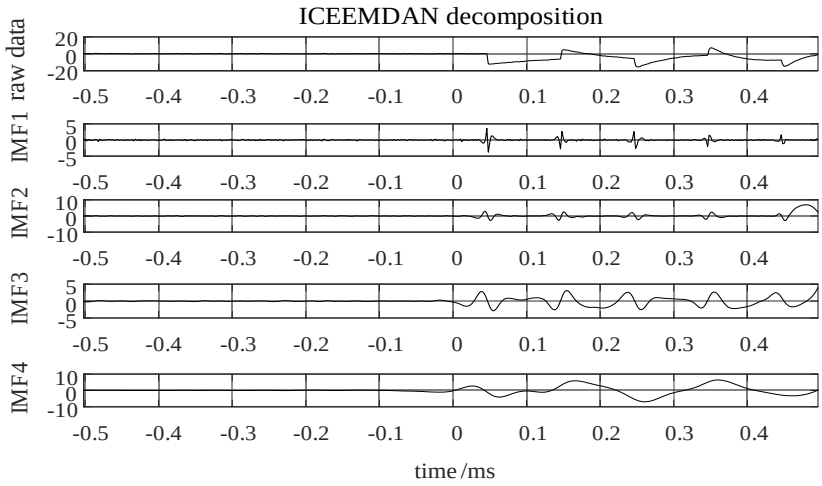


Figure 13: M-terminal ICEEMDAN decomposition results

The instantaneous energy spectrum of each IMF component is calculated using DEO3S. It is determined that the IMF1 component exhibits the highest energy peak-to-average ratio, and thus, it is identified as the primary frequency component. Consequently, the instantaneous energy spectrum of the IMF1 component is utilized for fault localization, with the point of maximum energy value serving as the calibration reference, as illustrated in Fig. 14.

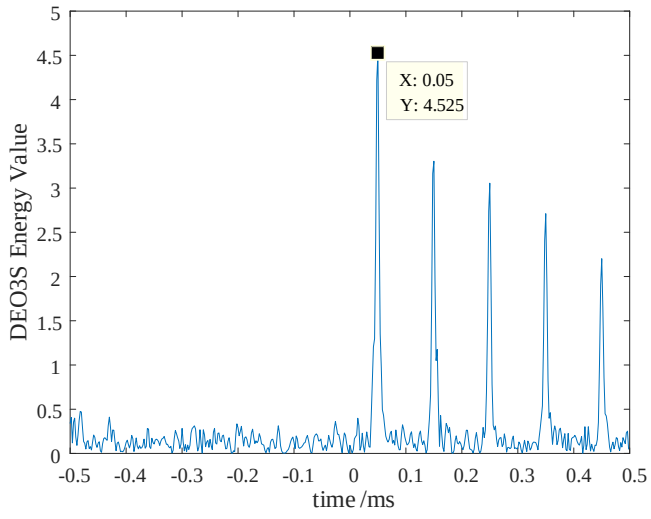


Figure 14: M-terminal DEO3S transient energy

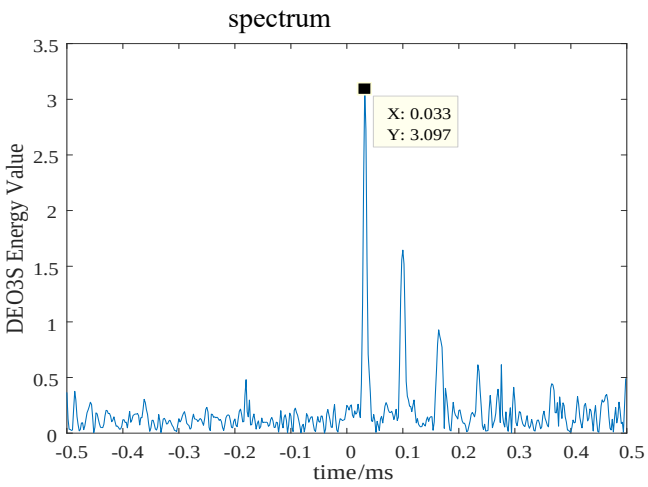


Figure 15: N-terminal DEO3S transient energy spectrum

Similarly, the instantaneous energy spectrum at the N-terminal is obtained as illustrated in Fig. 15.

From the traveling wave head position calibrated in Fig. 14 and Fig. 15, it can be observed that the arrival time t1 of the first traveling wave head at the M end is the first 0.05 ms, and the arrival time t2 of the first traveling wave head at the arrival time at the N end is the first 0.033 ms, and according to Eq. (9), the distance from the fault point to the M end is calculated to be 15.035 km. This indicates that the localization error is 35 m, which is within an acceptable range. Therefore, the localization is accurate.

### *C. Method Adaptation Analysis for Variations in Fault Distance and Transition Resistance*

In order to evaluate the adaptability of the proposed fault localization method in diverse fault scenarios, a fault simulation is conducted by establishing distinct fault distances and transition resistor faults, as illustrated in Fig. 9.

1) Variations in fault distance

In accordance with the typical fault cases outlined in subsection 4.2, the remaining fault conditions are maintained, with only the fault distance undergoing alteration. The distances from the four different fault locations (x1, x2, x3, and x4) to the M-terminal are 3 km, 9 km, 15 km, and 22 km, respectively. The corresponding measured voltages at the M-terminal are $U_{m1}$, $U_{m2}$, $U_{m3}$, and $U_{m4}$, respectively. As illustrated in Fig. 16, the corresponding voltages at the N-terminal are $U_{n1}$, $U_{n2}$, $U_{n3}$, and $U_{n4}$, as shown in Fig. 17.

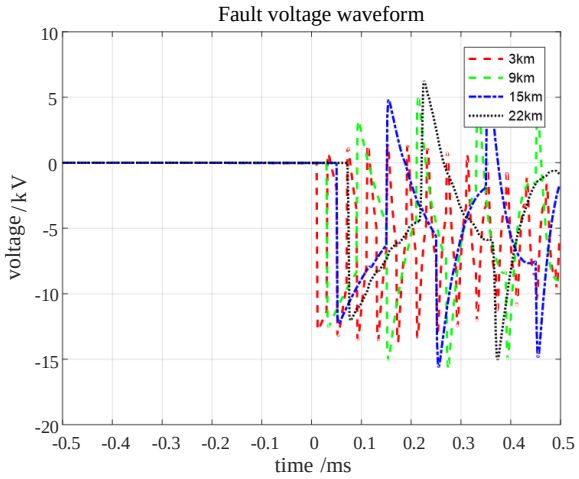


Figure 16: Voltage at M-terminal for different fault distances

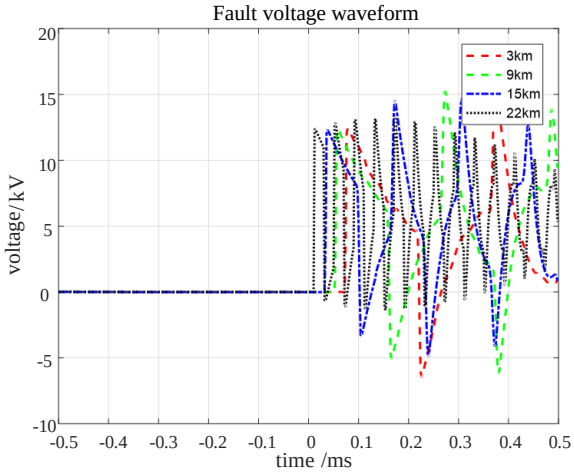


Figure 17: Voltage at N-terminal for different fault distances

As illustrated in Fig. 16 and Fig. 17, the greater the distance between the fault and the line, the later the arrival time of the traveling wave. The method proposed in the thesis is capable of extracting fault transient information for fault location by detecting the voltage waveforms of the current-limiting reactors at both ends of the line.

A small amount of noise is added to the aforementioned collected signals, and the transient energy spectrum corresponding to the aforementioned signals is calculated according to the fault localization process depicted in subsection B. The traveling wave head is calibrated, and the transient energy spectrum corresponding to the M and N terminals is shown in Fig. 18 and Fig. 19.

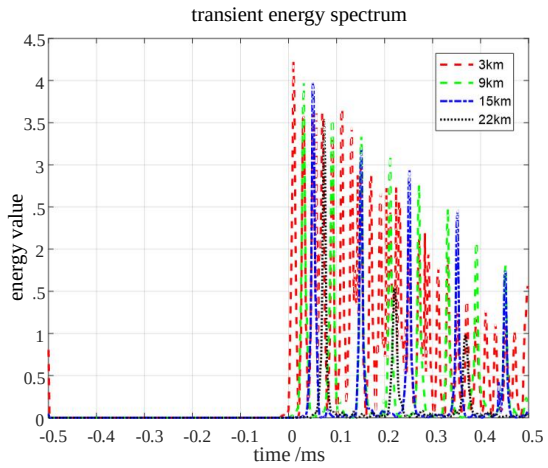


Figure 18: DEO3S instantaneous energy spectra for four faults at the M-terminus

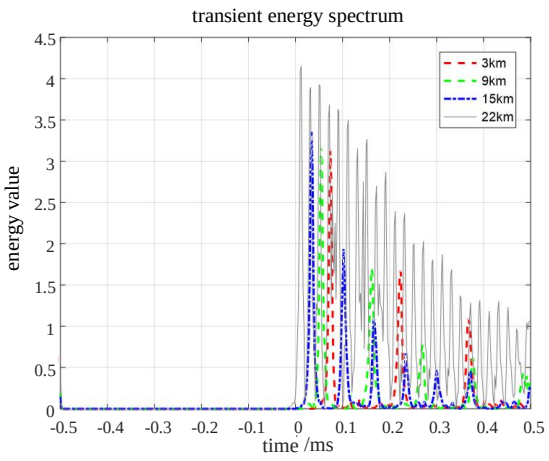


Figure 19: DEO3S instantaneous energy spectra for four faults at the N-terminus

The fault distance is calculated based on the calibrated traveling wave head time, and the resulting localization is presented in Table 2.

Table 2: Localization results for different fault distances

| Fault location | M-terminal wave-head calibration time(ms) | N-terminal wave-head calibration time(ms) | Fault location distance(km) | Inaccuracies(m) |
|---|---|---|---|---|
| x1 | 0.010 | 0.074 | 2.955 | 45 |
| x2 | 0.031 | 0.054 | 9.069 | 69 |
| x3 | 0.051 | 0.034 | 15.035 | 35 |
| x4 | 0.074 | 0.010 | 22.045 | 45 |

The results of the localization analysis presented in Table 2 demonstrate that the fault localization method proposed in this paper is capable of accurately localizing faults under varying distances.

2) Different transition resistances

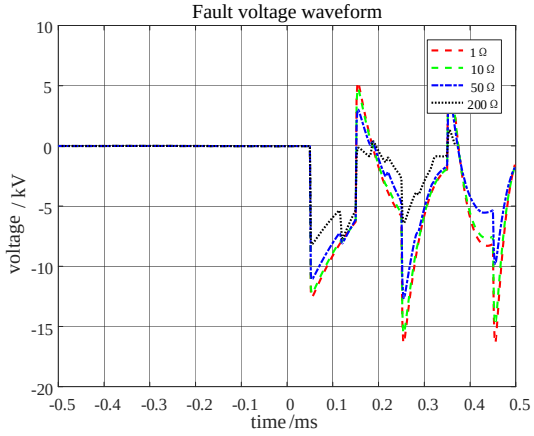


Figure 20: Voltage waveforms with different resistors at M

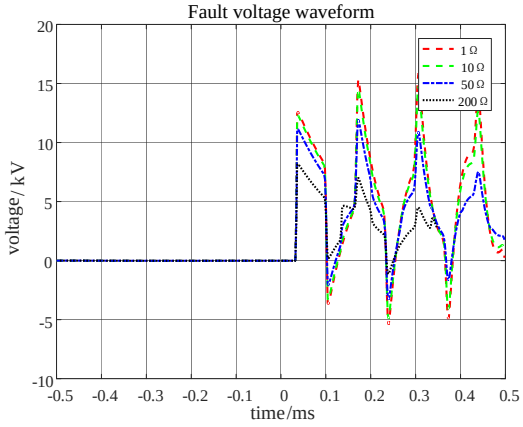


Figure 21: Voltage waveforms with different N-terminus resistors

In accordance with the typical fault case delineated in subsection B, the transition resistance of the faults is the sole variable, with the transition resistances of the four faults set to 1 Ω, 10 Ω, 50 Ω, and 200 Ω, respectively. The resulting measured voltages at the M-terminal are illustrated in Fig. 20, while those at the N-terminal are depicted in Fig. 21.

In accordance with the established methodology for fault localization, the instantaneous energy spectrum corresponding to the aforementioned signals is calculated and the traveling wave head is calibrated. The resulting instantaneous energy spectra at the M and N terminals are presented in Fig. 22 and Fig. 23, respectively.

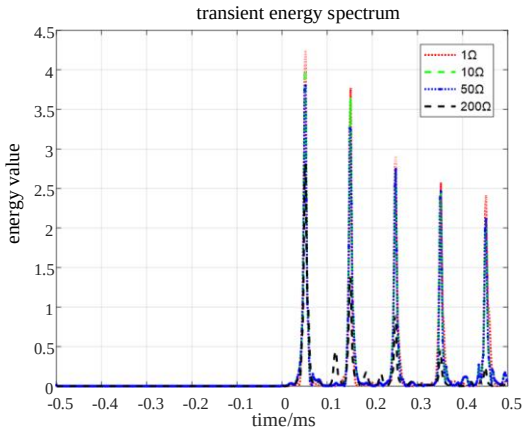


Figure 22: Instantaneous energy spectra of DEO3S corresponding to the four faults at the M-terminal side

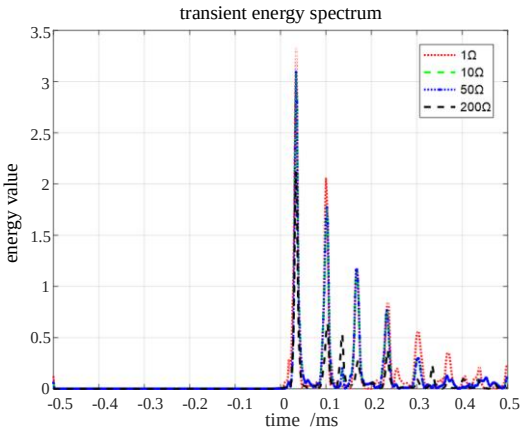


Figure 23: Instantaneous energy spectrum of DEO3S corresponding to four faults at the N-terminal side

As illustrated in Figs. 20 to Fig. 23, an increase in transition resistance is accompanied by a reduction in the amplitude of fault transient information and a more pronounced waveform distortion. However, the proposed method in this paper is still capable of accurate calibration of the first fault traveling wave head, even when the transition resistance reaches 200 Ω. The calibration time of the M-end wave head is the first 0.0. The localization result for the M-end wave head is 15.035 km, with an error of 35 m. The localization result for the N-end wave head is 0.034 ms, with an error of 35 m.

3) Different fault locations and transition resistances

To further verify the reliability and localization accuracy of the proposed method, a large number of fault cases with different fault locations and transition resistors were set up in Fig. 9 for simulation verification. The resulting fault localization results are shown in Table 3.

Table 3: Localization results for multiple fault cases

| Fault location | Reference terminal | Fault distance （km） | Fault resistance(Ω) | Fault location distance(km) | Inaccuracies(m) |
|---|---|---|---|---|---|
| $f_1$ | M-terminal | 5 | 200 | 5.050 | 50 |
| | | 8 | 50 | 8.030 | 30 |
| | | 14 | 20 | 13.990 | 10 |
| | | 21 | 10 | 20.993 | 7 |
| $f_2$ | N-terminal | 4 | 60 | 4.040 | 40 |
| | | 9 | 30 | 8.957 | 43 |
| | | 13 | 20 | 12.980 | 20 |
| | | 17 | 10 | 17.003 | 3 |
| $f_3$ | Q-terminal | 3 | 5 | 2.964 | 36 |
| | | 6 | 15 | 5.944 | 56 |
| | | 9 | 75 | 9.073 | 73 |
| | | 12 | 120 | 12.053 | 47 |
| $f_4$ | P-terminal | 3 | 1 | 2.997 | 3 |
| | | 7 | 30 | 7.020 | 20 |
| | | 13 | 80 | 12.980 | 20 |
| | | 18 | 200 | 18.046 | 46 |

According to equation (9), it can be calculated that when the sampling rate is 1 MHz, the error resulting from the lack of sampling rate is within ±75 m, and the errors of the localization results shown in Table 3 are all within ±75 m. This indicates that the fault localization method proposed in the paper is largely independent of the fault location and transition resistance. Furthermore, it can accurately calibrate the traveling wave head under the condition that the transition resistance is not higher than 200Ω, which is highly reliable and accurate in terms of localization.

### *D. Comparison and Analysis of Noise Resistance*

Given the potential for a considerable amount of noise to accompany faults in the actual DC distribution network, the paper aims to verify the reliability and accuracy of the proposed method for fault localization under noise conditions. To this end, the proposed method is subjected to simulation with the addition of Gaussian white noise, while a comparative analysis is conducted. Furthermore, the proposed method is analyzed in comparison to the "Wavelet Transform and ESMD Algorithm Based Fault Localization Methods" proposed in the literature [25] and the "VMD and TEO Algorithm Based Fault Localization Methods" proposed in the literature [26].

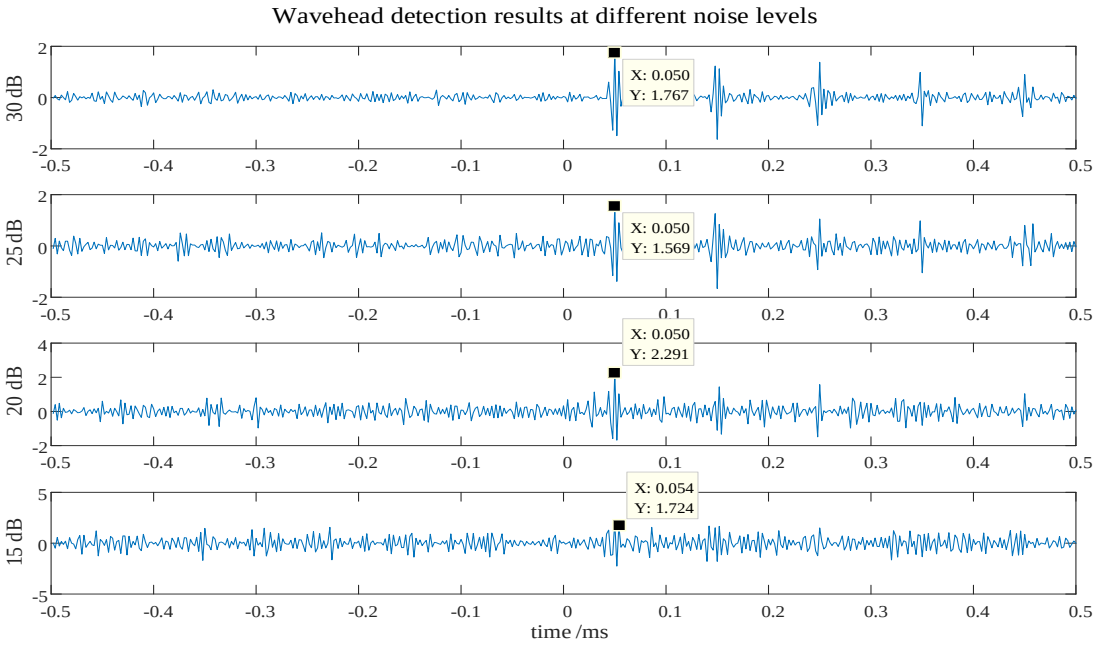


Figure 24: Detection results of the algorithm in literature [25] with noise

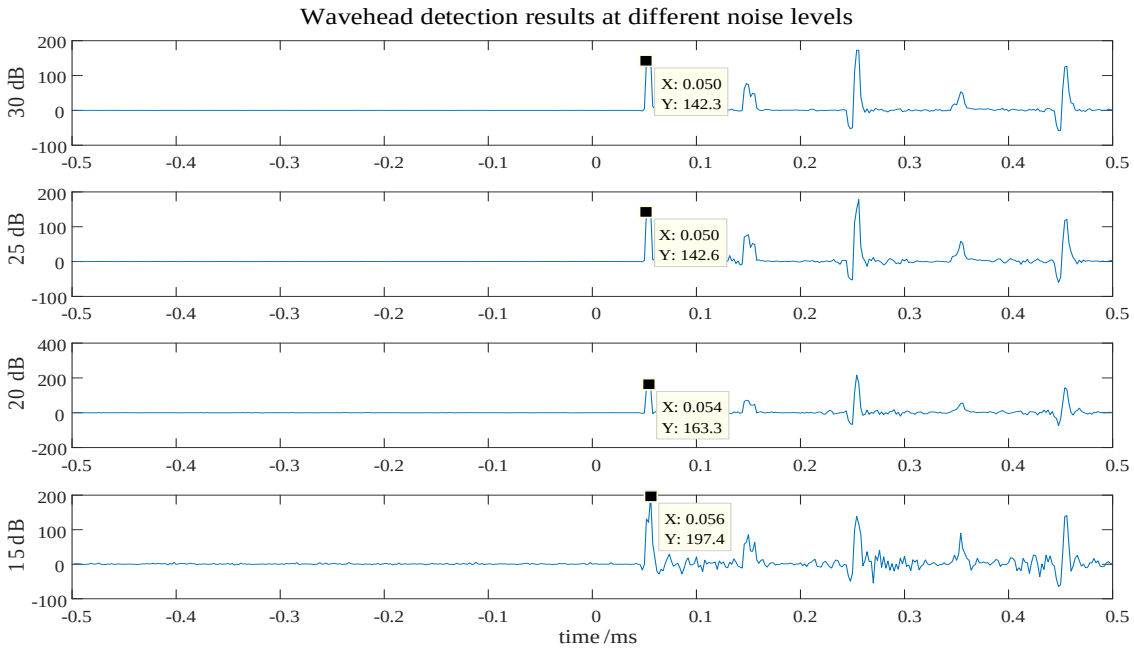


Figure 25: Detection results of the algorithm in literature [26] with noise

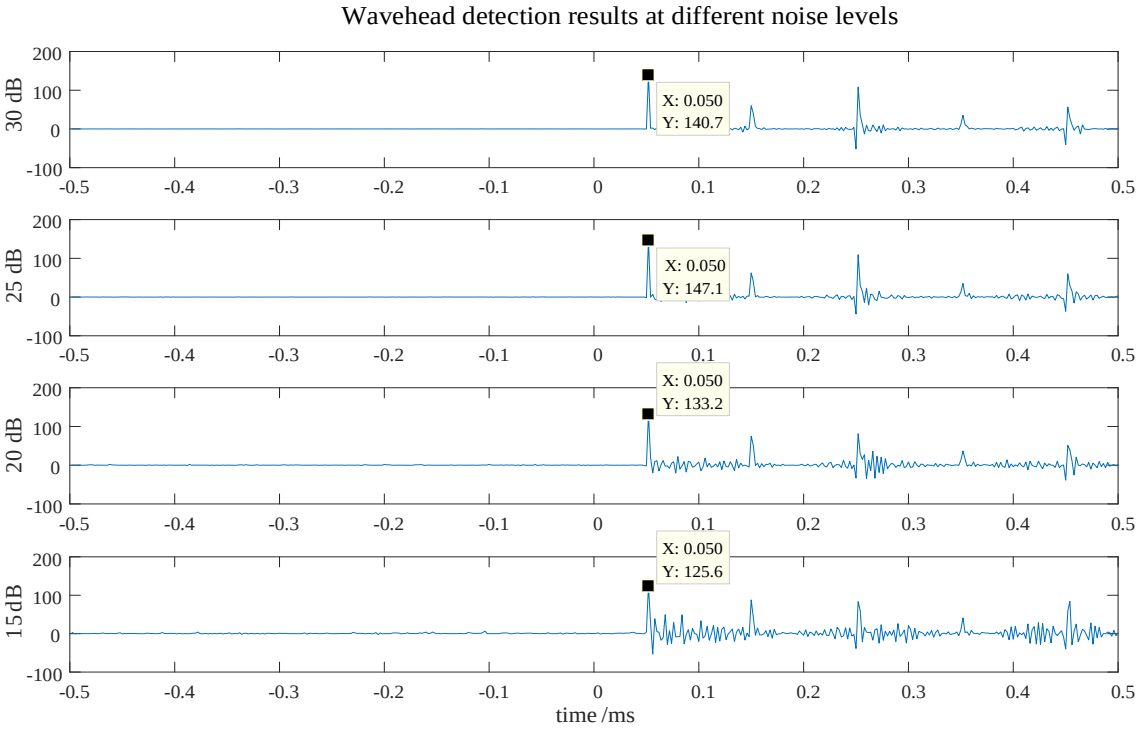


Figure 26: Results of the proposed algorithm in the presence of noise

The typical fault case presented in subsection B is utilized as a case study. Three distinct white noise interference signals, with levels of 30dB, 25dB, 20dB, and 15dB, respectively, are employed. These signals are subjected to wave-head detection through a variety of methodologies, with the outcomes presented in Fig. 24 to Fig. 26.

As illustrated in the accompanying figures, the algorithm proposed in the literature [25] is capable of accurately calibrating the wave-head when the noise is minimal. However, due to the wavelet algorithm's requirement for selecting the optimal basis function, its denoising ability is limited when the noise reaches 15 dB, which occurs when the wave-head has been completely submerged. This may result in inaccurate calibration of the wave-head, and in some cases, may even prevent the algorithm from recognizing the wave-head. The algorithm proposed in the literature [26] exhibits slightly enhanced noise immunity and is capable of effectively removing the majority of noise. However, the TEO algorithm is susceptible to the phenomenon of modal aliasing, which can result in inaccurate wave-head calibration in the case of 20dB and 15dB noise. This, in turn, can lead to significant errors in the results of fault localization. The ICEEMDAN-DEO3S algorithm proposed in the paper is capable of accurately calibrating the wave-head in the presence of significant noise

interference, with enhanced noise robustness and localization accuracy compared to the aforementioned algorithms. This makes it a more practical choice.

## VI. SUMMARY

This paper proposes a flexible DC distribution network fault localization method based on ICEEMDAN and DEO3S. The aim is to address the limitations of existing methods, which are affected by the initial traveling wave head calibration accuracy and noise. The proposed method is designed to overcome the inaccuracy and other problems associated with fault localization. To validate the effectiveness of the proposed localization method, a flexible DC distribution network line model is built in the PSCAD/EMTDC simulation environment. The proposed localization method was validated, and the following conclusions were drawn:

1) A flexible DC distribution network fault localization method based on ICEEMDAN and DEO3S is proposed. The ICEEMDAN algorithm is used to decompose the fault traveling wave, and the DEO3S algorithm is employed to discriminate the dominant frequency component of the fault traveling wave. The instantaneous energy spectrum is then extracted by the DEO3S algorithm. The highest energy point is regarded as the wave head of the fault traveling wave for the calibration and fault localization. This method optimizes the utilization of fault traveling wave transient information. The fault transient information of a 1 ms short time window can be employed to complete the fault localization. Furthermore, it enhances the calibration accuracy of the traveling wave head and noise immunity.

2) Simulation results demonstrate that the fault localization accuracy of this method is within 75 m, and it is not affected by fault distance, transition resistance, and high noise environment. Therefore, it has good applicability. Compared with existing DC distribution network fault traveling wave localization methods, the proposed method improves the localization accuracy while significantly improving the anti-noise ability, which improves the accuracy and reliability of DC distribution network fault localization and is more suitable for practical engineering applications.

## ACKNOWLEDGMENT

This work was supported by China Southern Power Grid Digital Power Grid Group Co., Ltd. This work was funded by the project of China Southern Power Grid Digital Power Grid Group Co., Ltd. (Number: 210002KK52222011).

## REFERENCES

[1] Shu Y. B. Study on the Promotion of Clean Energy Development by State Grid Corporation. Beijing, State Grid Corporation, 2010-03-09.

[2] Liu Z. Y. Research of Global Clean Energy Resource and Power Grid Interconnection [J]. Proceedings of the CSEE, 2016, 36(19): 5103- 5110+5391.

[3] Wen J. L., Wu R., Peng C., et al. Analysis of DC Grid Prospects in China [J]. Proceedings of the CSEE, 2012, 32(13): 7-12+185.

[4] Yao L. Z., Wu J., Wang Z. b., et al. Pattern Analysis of Future HVDC Grid Development [J]. Proceedings of the CSEE, 2014, 34(34): 6007-6020.

[5] Xin B. A. Contributing Wisdom and Strength to Realize the Goal of "Peak Carbon Achievement and Carbon Neutrality"[J]. State Grid, 2021(03): 2-3.

[6] Xin B. A., S. B. G., Li Q. H., et al. Rethinking of the "Three Elements of Energy" Toward Carbon Peak and Carbon Neutrality [J]. Proceedings of the CSEE, 2022, 42(09): 3117-3126.

[7] Development and Reform Commission's Guiding Opinions on Accelerating the Construction and Reconstruction of Distribution Grids [J]. Bulletin of the State Council of the People's Republic of China, 2016(03): 70-75.

[8] Zhang Z. Y., Lin P., Wang X. H. Review on relay protection of AC/DC hybrid distribution grids [J]. Power System Protection and Control, 2019, 47 (05): 179-187.

[9] Yang S. Z., Xiang W., Wen J. Y. Review of DC Fault Protection Methods for the MMC Based DC Grid [J]. Proceedings of the CSEE, 2019, 39(22): 6600-6617.

[10] Li B., He J. W., Feng Y. D., et al. Key Techniques for Protection of Multi-terminal Flexible DC Grid [J]. Automation of Electric Power Systems, 2016, 40(21): 2-12.

[11] Jia K., Li L., Xuan Z. W., et al. Study on fault location method and simulation for VSC-DC distribution network based on disturbance injection [J]. Power System Protection and Control, 2019, 47 (04): 99-106.

[12] Gao R. D., Wu Z. J., Fan W. C., et al. Line fault location method of VSC-based DC distribution system based on initial current differential value [J]. Electric Power Automation Equipment, 2018, 38 (02): 27-33.

[13] Li M., Jia K., Bi T., et al. Sixth harmonic-based fault location for VSC-DC distribution systems [J]. IET Generation, Transmission & Distribution, 2017, 11 (14): 3485-3490.

[14] He J. H., Zhang M., Luo G. M., et al. A Fault Location Method for Flexible DC Distribution Network Based on Fault Transient Process [J]. Power System Technology, 2017, 41 (03): 985-992.

[15] Song G. B., Li D. K., Chu X., et al. One-Terminal Fault Location for VSC-HVDC Transmission Lines Based on Principles of Parameter Identification [J]. Power System Technology, 2012, 36 (12): 94-99.

[16] Jia K, Li M, Bi T, et al. A voltage resonance-based single-ended online fault location algorithm for DC distribution networks [J]. Science China Technological Sciences, 2016, 59 (5): 721-729.

[17] Zhang Y. X., Wang H. D., Li T., et al. Combined Single-end Fault Location Method for LCC-VSC Hybrid HVDC Transmission Line [J]. Automation of Electric Power Systems, 2019, 43 (21): 187-194.

[18] Xu M. M., Xiao L.Y., Wang H.F., et al. Novel method of locating cable fault in DC distribution based on Prony algorithm [J]. Advanced Technology of Electrical Engineering and Energy, 2015, 34 (04): 1-5+30.

[19] Yang Y. C., Huang C., Wang X. Y., et al. A Novel Line Fault Location Method for DC Distribution Network [J]. Power System Technology, 2019, 43 (05): 1787-1794.

[20] Ma Z., Jiao Z. B., Li R. Network Structures and Key Technologies of DC Distribution Systems [J]. Power System Technology, 2017, 41 (10): 3348-3357.

[21] Lin F. W., Wu J. Y., Hao L. L. One-Terminal On-Line Fault Location Method for DC Distribution Cable Based on Apparent Pseudo-Impedance Identification [J]. Power System Technology, 2016, 40 (08): 2555-2561.

[22] Yin Z. L. , Chen Y. X. A new method for fault ranging and fault polarity identification based on flexible high-voltage DC transmission lines[J]. Electrotechnical Application, 2015, 34 (20): 75-78.

[23] Li D. K., Song G. B., Gao S. P., et al. Study on Automatic Fault Location for VSC-HVDC Transmission Lines Based on One-Terminal Traveling Wave [J]. Power System Technology, 2013, 37 (04): 1128-1133.

[24] Xu Y., Hu Z. Q., Dong H. R., et al. Fault Location Based on Comprehensive Grey Relational Degree for Flexible DC Distribution Network [J]. Acta Energiae Solaris Sinica, 2023, 44 (04): 324-331.

[25] Wang Y. W. The UHVDC Transmission Line Transient Protection and Fault Location Based on ESMD [D]. Kunming University of Science and Technology, 2016.

[26] Wang H. B., Zhou N. C., Wang W., et al. A double-terminal fault location method for UHVDC transmission lines based on traveling wave mode decomposition [J]. Power System Protection and Control, 2024, 52 (01): 109-120.